HHS Public Access

Author manuscript

Nat Struct Mol Biol. Author manuscript; available in PMC 2009 September 01.

Published in final edited form as:

Nat Struct Mol Biol. 2009 March ; 16(3): 265–273. doi:10.1038/nsmb.1566.

Structural and Functional Bases for Broad-Spectrum Neutralization of Avian and Human Influenza A Viruses

Jianhua Sui[1,*], **William C. Hwang**[2,*], **Sandra Perez**[3], **Ge Wei**[2], **Daniel Aird**[1], **Li-mei Chen**[3], **Eugenio Santelli**[2], **Boguslaw Stec**[2], **Greg Cadwell**[2], **Maryam Ali**[1], **Hongquan Wan**[3], **Akikazu Murakami**[1], **Anuradha Yammanuru**[1], **Thomas Han**[1], **Nancy J. Cox**[3], **Laurie A. Bankston**[2], **Ruben O. Donis**[3], **Robert C. Liddington**[2], and **Wayne A. Marasco**[1]

[1]Department of Cancer Immunology & AIDS, Dana-Farber Cancer Institute; Department of Medicine, Harvard Medical School, 44 Binney St. JFB 826, Boston, MA 02115, USA

[2]Infectious and Inflammatory Disease Center, Burnham Institute for Medical Research, 10901 North Torrey Pines Road, La Jolla, CA 92037, USA

[3]Influenza Division, Centers for Disease Control and Prevention, National Center for Immunization and Respiratory Diseases, 1600 Clifton Road - Mail Stop G-16 Atlanta, GA 30333, USA

Abstract

Influenza virus remains a constant public health threat, owing to its ability to evade immune surveillance through rapid genetic drift and reassortment. Monoclonal antibody (mAb)-based immunotherapy is a promising strategy for disease control. Here we use a human Ab phage display library and H5 hemagglutinin (HA) ectodomain to select ten neutralizing mAbs (nAbs) with a remarkably broad range among Group 1 influenza viruses, including the H5N1 “bird flu” and the H1N1 “Spanish flu” strains. Notably, nine of the Abs utilize the same germline gene, VH1-69. The crystal structure of one mAb bound to H5N1 HA reveals that only the heavy chain inserts into a highly conserved pocket in the HA stem, inhibiting the conformational changes

Correspondence should be addressed to J.S. (jianhua_sui@dfci.harvard.edu), R.O.D. (rvd6@cdc.gov), R.C.L (rlidding@burnham.org), and or W.A.M. (wayne_marasco@dfci.harvard.edu)..

*Contributed equally to the study.

Author Contributions DFCI team. J.S. and A.M. constructed H5-TH04 HA. J.S. and D.A. performed phage display Ab library selections and screening for Abs by ELISA, FACS and pseudo-viruses neutralization assays. J.S., M.A. and T.H. carried out epitope mapping using mutagenesis and FACS analysis. J.S., D.A. and M.A. purified antibodies. J.S. and A.Y. analyzed kinetics of Ab binding with HA protein. J.S performed HA subtype cross-binding and neutralization assay, pseudo-virus binding and fusion inhibition assay. J.S. and W.A.M designed the study, analyzed data, and wrote sections about these studies.
BIMR team R.C.L supervised all of the work done at BIMR. G.W. and G.C. cloned and expressed recombinant H5 for antibody panning and crystallization. W.C.H expressed F10 scFv and crystallized the F10-HA0 complex. W.C.H., E.S. and B.S. collected diffraction data and solved and refined the structure. L.A.B supervised cloning and expression. W.C.H., L.A.B and R.C.L. wrote sections about these studies.
CDC team. S.P.D., L.C., H.W. and R.O.D designed the study and performed animal study as well as virology study with wild type viruses. R.O.D wrote sections of these studies. J.S., R.O.D., R.C.L and W.A.M. finalized the paper. All authors commented on the manuscript.

Accession codes. Protein Data Bank: Coordinates and structure factors for the H5-F10 complex have been deposited with codes PDB ID 3FKU and RCSB ID RCSB050713.

The findings and conclusions in this report are those of the authors and do not necessarily represent the views of the Centers for Disease Control and Prevention or the Agency for Toxic Substances and Disease Registry.

required for membrane fusion. Our studies indicate that nAbs targeting this pocket could provide broad protection against both seasonal and pandemic influenza A infections.

Seasonal influenza A is a scourge of the young and old, killing more than 250,000 worldwide each year, while creating an economic burden for millions1. Pandemic influenza, which occurs when a new virus emerges and infects people globally that have little or no immunity, represents a grave threat to human health: for example, the 1918 “Spanish Flu” pandemic caused an estimated 50 million deaths2,3. Vaccines have historically been the mainstay of infection control. However, due to rapid antigenic drift, the vaccine antigen needs to be updated annually based on global influenza surveillance4,5, and it is not always fully successful. In addition, some recent H5N1 vaccines have shown promising results6-9, but none has been reported to elicit a broad neutralizing response in humans. Neuraminidase inhibitors, especially oseltamavir (Tamiflu), remain the primary antiviral treatment, but they have limited efficacy if administered late in infection, and widespread use is likely to result in the emergence of resistant viral strains10,11.

Influenza A is sub-classified by its two major surface proteins: hemagglutinin (HA or H), which mediates cell entry, first by recognizing host proteins bearing sialic acid on their surface, and second by triggering the fusion of viral and host membranes following endocytosis, allowing viral RNA to enter the cytoplasm; and neuraminidase (NA or N), which cleaves sialic acid from host and viral proteins, facilitating cell exit12. There are 16 HA subtypes and 9 NA subtypes which make up all known strains of influenza A viruses by various combinations of HA and NA12 (See Supplementary Fig. 1).

The recent spread of highly pathogenic avian influenza (HPAI), H5N1, across Asia, Europe and Africa raises the specter of a new pandemic, should the virus mutate to become readily transmissible from person-to-person. The evolution of H5N1 into a pandemic threat could occur through a single reassortment of its segmented genome or through the slower process of genetic drift12,13. Nearly 400 human H5N1 infections have been reported since 1997 from 14 countries, with a case mortality rate in the immunocompetent population above 60%4.

New therapeutic strategies that provide potent and broadly cross-protective host immunity are therefore a global public health priority. Human monoclonal antibody (mAb)-based “passive” immunotherapy is now being used to treat a number of human diseases, including Respiratory Syncytial Virus infection, and we have proposed how immunotherapy could be used strategically in a viral outbreak setting14.

In the present study, we first used a phage-display antibody library and recombinant H5 trimeric ectodomain to isolate a group of high-affinity neutralizing mAbs (“nAbs”) that were potent inhibitors of H5N1 viral infection *in vitro* and *in vivo*. Based on crystallographic and functional studies, we showed that the nAbs bind to a common epitope - a highly conserved pocket in the stem region of HA containing the “fusion peptide” - that rationalizes their ability to block membrane fusion rather than cell attachment. Sequence and structural analysis of all 16 HA subtypes points to the existence of just two variants of this epitope, corresponding to the two classic phylogenetic groupings of HA (Groups 1 and 2). We

therefore tested eight further Group 1 HA subtypes, and demonstrated a remarkable and unprecedented cross-subtype binding and/or neutralization spectrum. Since we had used a Group 1 subtype (H5) for our panning, our nAbs, as expected, failed to neutralize a Group 2 subtype, H7. These results nevertheless raise the possibility that a cocktail comprising a small subset of nAbs raised against representatives of the two groups could provide broad protection against all seasonal and pandemic influenza A viruses.

Results

Identification of nAbs against H5N1

The current H5N1 epidemics involve viruses derived from a single lineage of H5 HA. Within this lineage, four distinct clades have been identified as major threats to public health15,16. We expressed recombinant trimeric ectodomain of H5 HA from one of these viruses (strain A/Vietnam/1203/04 (H5N1), “H5-VN04”, Clade 1) in insect cells17 (Supplementary Fig. 2), immobilized it on a plastic surface, and selected Abs from a “non-immune” human Ab phage display library (utilizing single-chain VH-VL fragments (“scFv”))18. Two rounds of panning and the screening of 392 clones identified 10 unique Abs that were formed by six distinct VH (variable region of heavy chain) fragments in combination with seven different VL (variable region of light chain) fragments. (Supplementary Table 1).

We found that all 10 nAbs bound trimeric H5-VN04 with similar avidity, but did not bind monomeric HA1 (Fig. 1a). Presented as scFv-Fc constructs, they potently neutralized the Clade 1 H5 pseudo-virus, A/Thailand/2-SP-33/2004 (H5N1) (“H5-TH04”) (Fig. 1b); and, in a stringent plaque-reduction assay, they all exhibited high levels of neutralization against H5-VN04, as well as the more divergent (Clade 2.1) A/Indonesia/5/2005 (“H5-IN05”) (Fig. 1 c-d). We further found that the nAbs cross-competed with each other in a competition ELISA (Supplementary Fig. 3), suggesting that they share a common epitope. Based on this finding, as well as VH sequence diversity and neutralization potency, we converted three of the nAbs (D8, F10 and A66) into full-length human IgG1s for further studies; all three IgG1s bound to recombinant H5-VN04 with high affinity (Kd~100-200 pM) and very slow dissociation rates (kd ~ 10^{-4} s^{-1}) (Supplementary Fig. 4).

Prophylactic and therapeutic efficacy in mice

The protective efficacy of the three IgG1s against H5N1 virus infection was evaluated in a BALB/c mouse model (Fig. 2). Mice were treated with IgG1s before (prophylactically) or after (therapeutically) lethal viral challenge. Prophylaxis using 10 mg kg^{-1} of IgG1s effectively protected (80-100%) mice when challenged with a high lethal dose of H5-VN04 (Clade 1) or A/HongKong/483/97 (H5-HK97) (Clade 0) (Fig. 2a-b). Therapeutic treatment with 15 mg kg^{-1} (an achievable dose in humans) of IgG1 at 24h post-inoculation also protected 80-100% of the mice challenged with either H5-VN04 or H5-HK97 virus (Fig. 2c-d). Mice treated at later times (48 or 72h post-inoculation) with H5-VN04 showed similar or higher levels of protection (Fig. 2e-f). Furthermore, surviving mice remained healthy and showed minimal body weight loss over the 2-week observation period (data not shown).

While human influenza viruses are typically restricted to the upper respiratory tract, systemic spread is a typical outcome of H5N1 infection in mice, and has been reported in some humans. We found that the three IgG1s caused potent suppression of viral replication in the lungs (measured 4 days post-challenge) of mice treated within 48 hours of viral challenge; and that two IgG1s, F10 and A66, were effective when given at 72 hpi. The impact of antibody therapy on systemic infection was dramatically demonstrated by ≥ 1000-fold suppression of virus spread to the spleen, even when given 72 hpi (Supplementary Fig. 5). Suppression was also seen in the brain, but in this case systemic spread was too low in control animals for accurate quantitation.

nAbs inhibit cell fusion rather than receptor binding

Two ways in which anti-HA Abs can neutralize infection is by blocking the initial binding of HA to its cellular receptor (sialic acid) or by interfering with the subsequent step of HA-mediated virus-host membrane fusion, which occurs in acidic endosomes19,20. We found that none of the nAbs inhibited virus binding to cells (Fig. 3a) or hemagglutination of red blood cells (data not shown). However, we were able to show, using a model system of cell fusion, that the nAbs potently inhibited membrane fusion (Fig. 3b).

Structural characterization of the nAb epitope

In order to provide a structural basis for neutralization and to explore the prospects for developing even broader-spectrum therapeutics, we determined the crystal structure of F10 (as the scFv fragment) in complex with the H5 (H5-VN04) ectodomain (Fig. 4, and Supplementary Table 2). We used H5 activated by cleavage of the single chain precursor, HA0, into two polypeptides, HA1 and HA2. Cleavage leads to the partial burial of the "fusion peptide" (the first ~21 residues of each HA2) into the stem19,21, which also contributes to the formation of each of three hydrophobic "pockets" located below the large trimeric receptor-binding head. In the complex, one F10 nAb binds into each pocket, burying ~1500 Å2 of protein surface. Only the heavy chain (VH) participates directly in binding, utilizing all three of its complementarity-determining regions (CDRs). The light chain (VL) points out into solution, and makes only non-specific contacts with the distal end of the oligosaccharide of glycosylated residue $Asn33_1$ from a neighboring monomer. The epitope on H5 encompasses the entire pocket, which is formed by the HA2 fusion peptide, flanked by elements of HA1 on one side and helix αA of HA2 on the other.

The key interactions are as follows (Fig. 4b): (i) CDR-H2 adopts the "type 2" conformation22, which is relatively rare in human Abs. Two hydrophobic residues, Met54 and Phe55, from the tip of H2, insert into the pocket. Phe55 lies across a flat hydrophobic surface formed by the main-chain of the fusion peptide, residues 18_2-21_2; it also makes favorable orthogonal aromatic interactions23 with the side-chains of $Trp21_2$ at the back of the pocket, and $His18_1$ at the front (subscripts 1 or 2 refer to HA1 or HA2, and the numbering scheme follows the structure of H3 (pdb:2hmg)17,24). The Met54 sulfur makes II-aromatic interactions25 with the $Trp21_2$ ring, hydrophobic interactions with $Ile45_2$ from helix αA, an a H-bond between Met54 C=O and the $His38_1$ side-chain; s. (ii) Tyr102 from CDR-H3 extends from the apex of the H3 loop, to a location only ~3 Å from Phe55, and complements CDR-H2 by cementing together the fusion peptide (via a main-chain H-bond

to Asp19$_2$) and the αA helix of HA2 (by intercalating between Thr41$_2$ and Ile45$_2$). A large hydrophobic residue at the neighboring position 103 supports the side-chain conformation of Tyr102; and (iii) the CDR-H1 loop is characterized by small hydrophobic/polar side-chains (notably Val27, Thr 28 and Ser31) such that CDR-H1 fits snugly beneath the HA head while packing against helix αA. A somatic mutation of conserved Gly26=>Glu generates a non-canonical conformation for H1, with Thr27 pointing outward and making contact H5.

An N-terminal hairpin (residues I29$_2$ and M30$_2$) from HA2 of the counterclockwise neighbor packs against the other side of helix αA at this point, wrapping around its fusion peptide and further locking it into place (Fig. 4a and 4c). Thus, F10 may stabilize the fusion peptide of more than one subunit. One framework (FR3) residue, Gln74, appears to be especially important in stabilizing the CDR-H1 and CDR-H2 loop conformations, by forming H-bonds to the main chain C=O groups of Pro53 and Met54, as well as the side-chain of Ser30. The FR3 residue at position 72 is the major determinant of the choice between two distinct conformations of the H2 loop22.

Consistent with the structural data, mutations in three H5 residues on HA2 αA that make important interactions with F10 - Val52$_2$, Asn53$_2$ and Ile56$_2$ - greatly reduce or ablate nAb binding, while the conservative mutation, Val52Leu, has no effect (Fig. 4c-d). Mutations to other surfaces of the αA helix either have no effect (typically exposed residues) or lead to increased nAb binding, perhaps by subtly increasing the flexibility of the epitope (Fig. 4d). Significantly, the nine other nAbs show very similar mutant binding profiles. Together with the cross-competition noted above, this strongly suggests that the epitopes for all 10 nAbs overlap very closely indeed, and that the nAbs bind in a similar location and orientation.

Structural basis of H5 neutralization by the nAb panel

The broad neutralizing behavior against H5 may be attributed in part to the exclusive role of VH in antigen binding and the use of a common germline gene, VH1-69, in five out of the six VHs - although their CDR3 loops are variable in sequence and length (13-17 residues) (Supplementary Fig. 6 and Supplementary Table 1). In addition, free energy calculations26 point to dominant binding contributions (~70% of the total favorable free energy) of the three conserved residues in the VH segment (Fig. 5b). In CDR-H2 derived from germline V1-69, position 55 is always Phe, and position 54 is always hydrophobic (M/I/L/V). In our nAbs, CDR-H3 always has a Tyr predicted to lie at the tip of the CDR3 loop (conserved at the 6th position). The conformation and sequence of the CDR1 loop does not seem to be critical, since the other Abs we isolated do not contain the somatic mutation (Gly26=>Glu) found in F10, and are predicted to have canonical structures. The sixth VH gene we isolated is derived from the germline gene, VH1-2; its H2 loop has the same length as VH1-69, but by virtue of a change from Ala to Arg at position 7222 it is predicted to adopt a distinct conformation (“type 3”), which presents loop residues 3 and 4 to the antigen (rather than residues 4 and 5 in type 2 loops). The specific somatic mutation at position 4, from Asn to Met, presumably promotes H5 binding. It is not possible to predict the structure of the larger H3 loop, but a tyrosine is located at the center of the loop that may play an analogous role to that in VH1-69.

Thus, the F10-H5 crystal structure suggests a common mechanism of H5 virus neutralization for our nAb panel. They make no contact with the receptor-binding sites in the head and so do not inhibit cell attachment. Rather, they lock the fusion peptide and helix αA in place, thereby preventing the large structural reorganizations that are required for membrane fusion17,19,27-30. Our data point to this event occurring at an early step in the infectious process, although we cannot rule out the possibility that the nAbs act at a later stage, given the close packing of molecules on the surface of the mature virion which might restrict early access to the epitope. The only previously published crystal structure of an HA-nAb complex that inhibits membrane fusion utilizes a different mechanism: it prevents conformational changes by cross-linking the upper surfaces of adjacent subunits in the head31.

Anti-H5 nAbs bind and neutralize a broad range of Group 1 viruses *in vitro* and *in vivo*

Next, we examined all of the available HA sequences (total 6360) in the public influenza sequence database (Supplementary Table 3). Of note, the sequences of the F10 epitope are nearly always conserved within the H5 subtype. Indeed, many epitope residues, especially in HA2, are highly conserved across all 16 HA subtypes (Fig. 5). This high sequence conservation provides a rationale for the cross-neutralization of the H5N1 virus clades described above, and prompted us to test our antibodies against a broader range of HA subtypes.

Group 1 viruses, which contain 10 of the 16 subtypes, are further classified into 3 “clusters”, H1a, H1b, and H932,33 (Fig. 5). We tested nAb binding to eight members of Clusters H1a, H1b and H9, which include avian H5 as well as the most common human influenza subtypes (the major exception is the Group 2 subtype, H3). In addition to H5, we found that all three IgG1s bound to cells expressing full-length H1 from two different strains of H1N1, including the 1918 “Spanish flu”; H2 from H2N2; and H6 from H6N2; the Cluster 1b subtypes: H11 from H11N9; H13 from H13N6; and H16 from H16N3; as well as Cluster H9 subtypes from two H9N2 strains. However, none of them bound to a Group 2 subtype, H7 from H7N1 (Supplementary Fig.7).

The IgG1s also neutralized H5-, H1-, H2-, H6- and H11-pseudotyped virus infections (Fig. 6a). In a micro-neutralization assay, F10-IgG1 also neutralized H5N1, H1N1, H2N2, H6N1, H6N2, H8N4, and H9N2 influenza viruses (Fig. 6b). However, none of the nAbs neutralized Group 2 viruses, e.g. H3N2 (Fig. 6b and Supplementary Fig. 8). Thus, these nAbs recognize an epitope on HA that is conserved among H5 clades as well as in all members of Group 1 viruses. Finally, we demonstrated the *in vivo* protective efficacy of two of the IgG1s against two lethal H1N1 viral strains in a BALB/c mouse model, using the same protocol as for the H5N1 studies (Fig. 6c and d).

Structural basis of the Group-specific broad-spectrum virus neutralization

The ability of our nAbs to recognize all Group 1 (cluster H1a/b and H9) viruses (H12 was not tested) can be attributed to the key conserved features of the nAbs described above in combination with the highly conserved pocket on HA (Figs. 4 and 5). The epitope may be divided into 3 elements: (i) at its center, the sequence of the N-terminal segment of HA2 -

fusion peptide residues 18_2-21_2 - is conserved across all HA subtypes (note that the side-chain at position 19_2 does not participate in binding); (ii) a downstream segment of HA2 adopts part of the αA helix (residues 39_2-56_2), which is nearly invariant; the only significant difference is a Thr to Gln change at position 49_2 in the untested H9 cluster subtype, H12. $Thr49_2$ lies at the periphery of the epitope and makes one long H-bond (3.5 Å) to Ser31. Simple modeling suggests there is plenty of space to accommodate the larger Gln side-chain and that it can make comparable H-bonds; and (iii) smaller contributions from segments of the HA1 chain (residues 18_1 and 38_1) and a loop at the base of the head (residues 291_1 and 292_1).

3-dimensional comparisons of the epitope in the 5 known crystal structure subtypes (three Group 1 (H1, H5 and H9) and two Group 2 (H3 and H7) 21,32,34-36) show that they adopt two distinct structural classes consistent with the phylogenetic groupings32,33 (Fig. 7). These differences arise from group-specific differences in the location of buried residues, notably histidines ($H111_2$ is unique to Group 1; $H17_1$ is unique to Group 2) that have been proposed to be the “triggers” for pH-induced conformational changes29. The differences cause the side-chain of $Trp21_2$ to turn through 90° in Group 2 subtypes, eliminating favorable binding to Phe55 from our nAb panel. In addition, four out of six Group 2 subtypes are glycosylated at position 38_1, at the periphery of the F10 epitope; our modeling studies predict steric clashes with the CDR-H1 loop (data not shown). These structural differences rationalize the observed lack of binding/neutralization of Group 2 HA subtypes and viruses.

Prospects for Immune Escape

The remarkable transformation to the fusogenic state includes repacking of the central helices of three HA2 protomers to form a new triple-helical bundle, in which residues 34-37 form an N-terminal cap, as well as the creation of C-terminal arms that extend to the N-terminus of the new bundle37. It is straightforward to model the locations of the F10 epitope residues in this model of the fusogenic state (see Supplementary Note 1). All 8 epitope residues, which were fully exposed in the neutral pH structure, become either part of the new hydrophobic bundle core ($Thr41_2$, $Ile45_2$, $Val52_2$ and $Ile56_2$), or they make networks of H-bonds with the C-terminal arms and other elements that stabilize the new bundle (Lys 38_2, $Gln42_2$, $Thr49_2$, $Asn53_2$). The requirement for adopting two entirely different conformations, each with a distinct hydrophobic core and H-bonding network may place powerful evolutionary constraints on the sequence of the helix, as evidenced by the almost complete lack of genetic drift within helix αA among the 16 HA subtypes.

To test this hypothesis, we attempted to select neutralization escape mutants. We propagated VN/04 (H5N1) virus in MDCK cells for 72h in the presence of 40 μg ml^{-1} of each of the 3 nAbs as well as a murine Ab, 22F, that targets the receptor-binding head. Following three *in vitro* passages, we readily isolated a mutant VN04 virus (K193E) that was resistant to 22F. In contrast, we failed to identify any viruses resistant to any of our 3 IgG1s (D8, F10, or A66). While these experiments cannot prove that escape mutants with unimpaired viral fitness will never arise, they clearly support the notion that the pocket is more refractory than epitopes in the head. Notwithstanding, if such mutants should arise, we can employ our

in vitro approach to find new reactive nAbs, or further engineer the existing nAbs to have even broader spectrum reactivity38.

Discussion

Prior to the present study, the vast majority of nAbs isolated against influenza A virus have targeted the receptor-binding head and lacked broad cross-neutralizing activity. However, a murine nAb, termed C17939, was positively selected on the basis of its cross-neutralization properties (of H1 and H2 subtypes), and subsequently shown to neutralize H5, but not Group 2 subtypes39,40 (Supplementary Note 2). Moreover, C179 was shown to block membrane fusion rather than cell attachment and to protect mice against viral challenge41, although a detailed mechanism was not reported. We compared the activities of C179 and F10 and found that both showed similar binding towards H5. We also found that F10 efficiently competed with C179 for binding to H5, but not *vice versa* (Supplementary Fig. 9). Furthermore, the point mutant $V52_2E$ abrogated binding to both Abs, while $T318_1K$ only affected C179 binding. These results suggest that F10 and C179 have partially overlapping epitopes and that their modes of action are similar.

The manner in which HA was presented to the antibody phage display library in this study seems to have been critical in our success, since similar attempts to isolate broadly nAbs using cell-surface expressed HA showed only partial success against H5, and most Abs recognized linear epitopes42. As noted above, we repeatedly isolated nAbs that utilize the same VH germline gene (IGHV1-69 or “VH1-69”). Huang et al.43 have pointed out that this is the only VH gene that consistently encodes 2 hydrophobic residues at the tip of its CDR-H2 loop; indeed, it is the only germline gene to encode a Phe at this position, which makes several critical interactions with H5. Moreover, the “type 2” H2 loop, which is long and compact, is only predicted to occur in 4 out of the ~50 human germline genes. These factors may explain at least in part the remarkable ability of nAbs derived from this germline gene to cross-react with viral epitopes: their unusual ability to bind to conserved hydrophobic pockets. Such pockets are likely to have an important function and for this reason they are often cryptic in the unactivated state of the antigen. For example, VH1-69 is the predominant gene utilized by a group of CD4-induced (“CD4i”) nAbs raised against the HIV-1 surface glycoprotein, gp120, where the “pocket” is part of a conserved co-receptor binding site that is only exposed transiently upon binding to its primary receptor, CD443. Similarly, an antibody raised against the HIV gp41 trimeric “inner-core” fusion protein intermediate utilizes the hydrophobic tip of its VH1-69 CDR-H2 loop to insert into a conserved hydrophobic pocket that blocks further assembly to the fusion-competent 6-helix structure44. *In vivo*, B cells carrying the VH1-69 gene are the primary mediators of innate defense against HCV infection, generating antibodies against its membrane fusion glycoprotein, E245, although the epitope and mode of action have not been determined. Notably, as we found in the current study, VH1-69 is not the only germline that is suitable for achieving neutralization in a similar manner. Another recent example is a nAb against Ebola virus surface glycoprotein, KZ52, which uses the VH3-21 germline46. However, their common ability to lock viral envelope proteins into a non-fusogenic conformation offers support for the possibility of a general strategy for broad-spectrum and/or potent viral neutralization.

Recent work using immune-based phage-display libraries generated from B cell populations of patients who survived H5N1 infection resulted in the isolation of three human nAbs that neutralized both H1 and H5 viral strains. The authors postulated that the reason for survival was an effective humoral immune response mediated by such nAb-generating B cells *in vivo*47, although no control populations were studied. Analysis of their data (Supplementary Note 3) indicates that the antibodies are also derived from the VH1-69 germline gene, and share other key characteristics, including the Met-Phe pair in CDR-H2 and a tyrosine at the tip of CDR-H3. Thus it would appear, at least in this case, that our non-immune (H5-naive) donor library approach generated antibodies with characteristics very similar to those found using immunized-donor-based phage-display libraries derived from H5N1 survivors.

Why broad-spectrum nAbs similar to those identified in our study are not similarly generated/expanded during successive rounds of influenza infection and repeated vaccination is not known (Supplementary Note 4), and warrants further investigation. It is unlikely that the F10 epitope provokes self-tolerance mechanism(s) via auto-antigen mimicry48 (Supplementary Note 5). Rather, we hypothesize that an immunodominant Ab response to the highly-exposed globular head may overwhelm the Ab response to the F10-epitope, although it remains possible that other immune exclusion mechanism(s) may preclude natural Ab responses against the F10 epitope. It is not surprising that many viruses are highly adept at keeping their most critical (and conserved) determinants of pathogenesis cryptic, in which case subunit-based vaccines, utilizing properly presented fragments of F10 or F10-like epitopes, may offer distinct advantages over whole-virus-based approaches for the induction of broad spectrum nAbs *in vivo*49,50.

In summary, we have used *in vitro* methodologies to isolate a family of high affinity broad-spectrum human nAbs against HA that show potent *in vitro* and *in vivo* efficacy against both highly pathogenic H5N1s and H1N1s. We show that they inhibit the post-attachment fusion process by recognizing a highly conserved epitope within the stem region of HA at a point where key elements of the conformational change are brought into close apposition. Our initial experiments suggest that this region is recalcitrant to the generation of escape mutants. The prospects for their use for passive immunotherapy would therefore seem to be excellent, either alone or in combination with small molecule inhibitors (Supplementary Note 6). Finally, our structural work pinpoints the reasons why Group 2 HAs do not bind the nAbs described here: despite surface sequence similarities, they form a structurally distinct group, but one that is also highly conserved and therefore may be amenable to a similar panning discovery approach.

Methods

Crystallization of the H5-F10 complex

H5-F10 complexes were formed by incubating the two purified components with an excess of F10 (See Supplementary methods), and isolated by Superdex 200 in TBS buffer. Peak fractions were pooled and concentrated to ~11 mg ml^{-1}. The integrity of the H5 trimer was examined using Gel filtration and SDS-PAGE. Crystals grew at 22°C by equilibrating equal volumes of protein and reservoir solution (12.5% PEG 1K (w/v), 25% ethylene glycol (w/v), 100 mM Tris, pH 8.5) using the hanging drop vapor diffusion technique.

Data collection, structure determination, and refinement

Diffraction data were collected from crystals flash-frozen at 100K in the reservoir buffer at the Stanford Synchrotron Radiation Laboratory beam-line 9.2, set at a wavelength of 1.0 Å, and processed with XDS51 and HKL200052. The structure was solved at 3.2 Å resolution by molecular replacement with PHASER using the structures of H5 (A/Vietnam/1194/04; PDB code 2IBX) and a homology model of F10 based on the structure of SARS nAb 80R (PDB code 2GHW)53,54 as starting models. The asymmetric unit contains two H5 trimers and three F10 molecules per trimer, and was refined using REFMAC555 with simulated annealing in CNS55 and manual rebuilding with Coot56 and Xtalview57. The final maps are of high quality, and key features such as the F10 CDR loops and interfacial residues are unambiguous and consistent in the 6 copies. The final model includes 503/503/503/497/497/497 residues for the 6 independent copies of H5, 235/235/236/233/234/234 residues for the 6 F10scFvs, 24 N-acetyl-D-glucosamine and 6 β-D-mannose units, but no water molecules. The R_{FREE} is .29 with excellent geometry as assessed with PROCHECK58 and Rampage (Table 1): percentage of residues in favored, allowed and outlier regions are 90.0%, 9.5%, and 0.5%, respectively.

Phage display library selection

We produced recombinant trimeric H5-VN04 ectodomain as for crystallization studies (see below) except that furin co-infection to ensure complete activation was not employed. Abs were identified by two-rounds of selection of a 27 billion member human scFv phage display library against recombinant trimeric H5 immobilized on Immunotube (Nunc), followed by ELISA screening. Ten unique anti-H5 Abs were identified by sequence analysis of 97 H5-positive clones out of 392 clones screened.

Plaque reduction assay

H5-VN04, H5-IN05 or A/Netherland/219/03 (H7N7) (H7-NL03) viruses (10,000 pfu) were incubated with anti-H5 scFv-Fcs at three different concentrations (1, 10 or 100 μg mL^{-1}) at 37°C for 30 mins. The virus-Ab mixture was diluted logarithmically and transferred onto MDCK cell monolayers in 12-well plates and incubated at 37°C for 1h. Cells were then washed and overlaid with agar. After 4 days of incubation, the overlay was discarded, and plaques visualized by crystal violet staining.

Microneutralization assay

The method was performed as described previously59. Briefly, 100 $TCID_{50}$ (median tissue culture infectious doses) of virus were mixed in equal volume with two-fold serial dilutions of Ab stock solution (0.1mg ml^{-1}) in 96-well tissue culture plates, and incubated for 1h at 37°C. Indicator MDCK cells (1.5×10^4 cells per well) were added to the plates, followed by incubation at 37°C for 20h. To establish the endpoint, cell monolayers were then washed with PBS, fixed in acetone, and viral antigen detected by indirect ELISA with a mAb against influenza A NP (A-3, Accurate).

Viral binding inhibition assay

0.5×10^6 293T cells were incubated with H5-TH04-pseudotyped HIV viruses (~ 500 ng of p24) in the presence of anti-H5 nAbs, control mAbs, or in the absence of antibodies, in PBS buffer containing 0.5% (w/v) BSA and 0.02% (w/v) NaN_3 at 4°C. After 1h incubation, cells were spun down. Supernatants were collected and tested for p24 levels using an HIV-1 $p24^{CA}$ capture ELISA kit (NCI, Frederick, NIH) to quantify unbound virus. Cells were then washed once or twice and lysed to quantify the cell-bound virus using the same method.

Cell fusion inhibition assay

HeLa cells, ~90% confluent in six-well plates, were transfected with pcDNA3.1-H5-TH04 plasmid (3 μg total DNA per well) using lipofectamine 2000 (Invitrogen). After ~30 hours of transfection, the culture medium was supplemented with 1 ml of anti-H5 or control mAbs for 1-2 hours, and cells were then washed and incubated with low-pH fusion buffer (150 mM NaCl +10 mM HEPES, adjusted to pH 5.0) for 4-5 mins. Cells were then returned to the standard culture medium for 2-3 hours at 37°C, and finally fixed with 0.25% (v/v) glutaraldehyde and stained with 0.1% (w/v) crystal violet. Photomicrographs were taken at 10× magnification.

Prophylactic and therapeutic efficacy studies in mice

Female 8-10 weeks old BALB/c mice were used in all experiments. Mice were weighed on the day of virus challenge and then daily for 2 weeks. Body weight was used as the clinical endpoint; mice with body weight loss ≥ 25% of pre-infection values were euthanized. Animal studies were conducted per approved Institutional Animal Care and Use Committee protocols.

Prophylactic efficacy study

Three human nAbs (D8-IgG1, F10-IgG1 and A66-IgG1) or control human mAb 80R-IgG118 at 2.5 mg kg^{-1} or 10 mg kg^{-1} were administered into 4 groups of 5 mice each by i.p. injection in 0.5 mL volume. One hour after mAb administration, two groups of mice were challenged with H5-VN04 and two groups with H5-HK97 by i.n. inoculation with 10 MLD_{50} in 50 μl volumes per mouse. Mice were observed and weighed daily for two-weeks after infection. Analogous studies were performed to evaluate the protective efficacy of the nAbs against A/Puerto Rico/8/1934 (H1N1) or A/WSN/1933 (H1N1) viruses.

Post-exposure therapy efficacy study

The experimental design recapitulates the prophylaxis study, with the following exceptions. Twelve groups of 10 mice were first inoculated i.n. with 10 MLD_{50} of VN04. At 24, 48 and 72 hours after H5-VN04 infection, one group of mice received i.p injections of 15 mg kg^{-1} body weight of one of the three nAbs or control (80R).

Supplementary Material

Refer to Web version on PubMed Central for supplementary material.

Acknowledgements

We wish to thank Dr. Judith Appleton (Cornell University, New York, USA) for a gift of mouse mAbs against H5N1, 17A2.1.2 and 22F; Dr. Alexander Klimov (CDC, Atlanta, USA) and Amanda Balish (CDC, Atlanta, USA) for providing ferret antiserum and virus sequences; Dr. Robert Webster (St. Jude Children's Research Hospital, Memphis, USA) for H11N9, H13N6 and H16N3 viral specimens; Dr. Le Quynh Mai (National Institute of Hygiene and Epidemiology, Vietnam Ministry of Health) for providing H5N1, Dr. Wilina Lim (Hong Kong Department of Health) for providing H5N1 and H9N2, as well as Endang Sedyaningsih, Triono Soendoro (National Institute of Health Research and Development, Indonesian Ministry of Health, Jakarta, Indonesia) for providing H5N1 specimens; Dr. Peter Palese (Mount Sinai School of Medicine, New York, USA) for providing pCAGGS-H1(SC) plasmid encoding full-length HA protein of H1-SC1918; Dr. Michael Farzan (New England Primate Research Center, Harvard Medical School, Boston, USA) for pCAGGS-H1 (PR) plasmid encoding HA protein of H1-PR34; Dr. Xinzhen Yang (Beth Israel Deaconess Medical Center, Harvard Medical School, Boston, USA) for pCAGGS-H7 (FPV) encoding H7-FP34 HA. We thank Drs. Wen Yuan and Wenhui Li for helpful discussions; Dr. Yaqiong Lin for assistance in crystallization and critical discussion. We thank the NIH and DOE for access to the Stanford Synchrotron Radiation Facility, and the facility staff for helping in X-ray data collection. Molecular graphics images were produced using the UCSF Chimera package from the Resource for Biocomputing, Visualization, and Informatics at the University of California, San Francisco (supported by NIH P41 RR-01081). This work was supported by NIH (U01-AI074518-01) to W.A.M. and in part by NIH (P01-AI055789) to R.C.L.

References

1. W.H.O. World Health Organization factsheet 211: influenza. 2003http://www.who.int/mediacentre/factsheets/2003/fs211/en/
2. Webster RG. 1918 Spanish influenza: the secrets remain elusive. Proc Natl Acad Sci U S A. 1999; 96:1164–6. [PubMed: 9989993]
3. de Wit E, Fouchier RA. Emerging influenza. J Clin Virol. 2008; 41:1–6. [PubMed: 18340670]
4. W.H.O. 2008http://www.who.int/csr/disease/influenza/influenzanetwork/en/index.html.
5. Carrat F, Flahault A. Influenza vaccine: the challenge of antigenic drift. Vaccine. 2007; 25:6852–62. [PubMed: 17719149]
6. Cinatl J Jr. Michaelis M, Doerr HW. The threat of avian influenza A (H5N1). Part IV: Development of vaccines. Med Microbiol Immunol. 2007; 196:213–25. [PubMed: 17541633]
7. Subbarao K, Luke C. H5N1 viruses and vaccines. PLoS Pathog. 2007; 3:e40. [PubMed: 17335350]
8. Leroux-Roels I, et al. Broad Clade 2 Cross-Reactive Immunity Induced by an Adjuvanted Clade 1 rH5N1 Pandemic Influenza Vaccine. PLoS ONE. 2008; 3:e1665. [PubMed: 18301743]
9. Baras B, et al. Cross-Protection against Lethal H5N1 Challenge in Ferrets with an Adjuvanted Pandemic Influenza Vaccine. PLoS ONE. 2008; 3:e1401. [PubMed: 18167560]
10. de Jong MD, et al. Oseltamivir resistance during treatment of influenza A (H5N1) infection. N Engl J Med. 2005; 353:2667–72. [PubMed: 16371632]
11. W.H.O. Clinical management of human infection with avian influenza A (H5N1) virus. http://www.who.int/csr/disease/avian_influenza/guidelines/ClinicalManagement07.pdf
12. Wright, P.; Neumann, G.; Kawaoka, Y. Orthomyxoviruses. In: Knipe, D.; Howley, P.; Griffin, D.; Lamb, R.; Martin, M., editors. Fields Virology. Vol. Vol. 2. Lippincott Williams; Wilkins: 2006. p. 1692-1740.
13. Fauci AS. Pandemic influenza threat and preparedness. Emerg Infect Dis. 2006; 12:73–7. [PubMed: 16494721]
14. Marasco WA, Sui J. The growth and potential of human antiviral monoclonal antibody therapeutics. Nat Biotechnol. 2007; 25:1421–34. [PubMed: 18066039]
15. W.H.O. 2007http://www.who.int/csr/disease/avian_influenza/guidelines/summaryH520070403.pdfhttp://www.who.int/csr/disease/avian_influenza/guidelines/summaryH520070403.pdf
16. W.H.O. Evolution of H5N1 avian influenza viruses in Asia. Emerg Infect Dis. 2005; 11:1515–21. [PubMed: 16318689]
17. Stevens J, et al. Structure and receptor specificity of the hemagglutinin from an H5N1 influenza virus. Science. 2006; 312:404–10. [PubMed: 16543414]

18. Sui J, et al. Potent neutralization of severe acute respiratory syndrome (SARS) coronavirus by a human mAb to S1 protein that blocks receptor association. Proc Natl Acad Sci U S A. 2004; 101:2536–41. [PubMed: 14983044]
19. Skehel JJ, Wiley DC. Receptor binding and membrane fusion in virus entry: the influenza hemagglutinin. Annu Rev Biochem. 2000; 69:531–69. [PubMed: 10966468]
20. Kida H, Yoden S, Kuwabara M, Yanagawa R. Interference with a conformational change in the haemagglutinin molecule of influenza virus by antibodies as a possible neutralization mechanism. Vaccine. 1985; 3:219–22. [PubMed: 4060852]
21. Ha Y, Stevens DJ, Skehel JJ, Wiley DC. H5 avian and H9 swine influenza virus haemagglutinin structures: possible origin of influenza subtypes. Embo J. 2002; 21:865–75. [PubMed: 11867515]
22. Chothia C, et al. Structural repertoire of the human VH segments. J Mol Biol. 1992; 227:799–817. [PubMed: 1404389]
23. Samanta U, Pal D, Chakrabarti P. Packing of aromatic rings against tryptophan residues in proteins. Acta Crystallogr D Biol Crystallogr. 1999; 55:1421–7. [PubMed: 10417410]
24. Weis WI, Brunger AT, Skehel JJ, Wiley DC. Refinement of the influenza virus hemagglutinin by simulated annealing. J Mol Biol. 1990; 212:737–61. [PubMed: 2329580]
25. Pal D, Chakrabarti P. Non-hydrogen bond interactions involving the methionine sulfur atom. J Biomol Struct Dyn. 2001; 19:115–28. [PubMed: 11565843]
26. Champ PC, Camacho CJ. FastContact: a free energy scoring tool for protein-protein complex structures. Nucleic Acids Res. 2007; 35:W556–60. [PubMed: 17537824]
27. Stevens J, et al. Structure of the uncleaved human H1 hemagglutinin from the extinct 1918 influenza virus. Science. 2004; 303:1866–70. [PubMed: 14764887]
28. Daniels RS, et al. Fusion mutants of the influenza virus hemagglutinin glycoprotein. Cell. 1985; 40:431–9. [PubMed: 3967299]
29. Thoennes S, et al. Analysis of residues near the fusion peptide in the influenza hemagglutinin structure for roles in triggering membrane fusion. Virology. 2008; 370:403–14. [PubMed: 17936324]
30. Earp LJ, Delos SE, Park HE, White JM. The many mechanisms of viral membrane fusion proteins. Curr Top Microbiol Immunol. 2005; 285:25–66. [PubMed: 15609500]
31. Barbey-Martin C, et al. An antibody that prevents the hemagglutinin low pH fusogenic transition. Virology. 2002; 294:70–4. [PubMed: 11886266]
32. Russell RJ, et al. H1 and H7 influenza haemagglutinin structures extend a structural classification of haemagglutinin subtypes. Virology. 2004; 325:287–96. [PubMed: 15246268]
33. Fouchier RA, et al. Characterization of a novel influenza A virus hemagglutinin subtype (H16) obtained from black-headed gulls. J Virol. 2005; 79:2814–22. [PubMed: 15709000]
34. Gamblin SJ, et al. The structure and receptor binding properties of the 1918 influenza hemagglutinin. Science. 2004; 303:1838–42. [PubMed: 14764886]
35. Yamada S, et al. Haemagglutinin mutations responsible for the binding of H5N1 influenza A viruses to human-type receptors. Nature. 2006; 444:378–82. [PubMed: 17108965]
36. Ha Y, Stevens DJ, Skehel JJ, Wiley DC. X-ray structure of the hemagglutinin of a potential H3 avian progenitor of the 1968 Hong Kong pandemic influenza virus. Virology. 2003; 309:209–18. [PubMed: 12758169]
37. Chen J, Skehel JJ, Wiley DC. N- and C-terminal residues combine in the fusion-pH influenza hemagglutinin HA(2) subunit to form an N cap that terminates the triple-stranded coiled coil. Proc Natl Acad Sci U S A. 1999; 96:8967–72. [PubMed: 10430879]
38. Sui J, et al. Broadening of neutralization activity to directly block a dominant antibody-driven SARS-coronavirus evolution pathway. PLoS Pathog. 2008; 4:e1000197. [PubMed: 18989460]
39. Okuno Y, Isegawa Y, Sasao F, Ueda S. A common neutralizing epitope conserved between the hemagglutinins of influenza A virus H1 and H2 strains. J Virol. 1993; 67:2552–8. [PubMed: 7682624]
40. Smirnov YA, et al. An epitope shared by the hemagglutinins of H1, H2, H5, and H6 subtypes of influenza A virus. Acta Virol. 1999; 43:237–44. [PubMed: 10749369]

41. Smirnov YA, Lipatov AS, Gitelman AK, Claas EC, Osterhaus AD. Prevention and treatment of bronchopneumonia in mice caused by mouse-adapted variant of avian H5N2 influenza A virus using monoclonal antibody against conserved epitope in the HA stem region. Arch Virol. 2000; 145:1733–41. [PubMed: 11003481]
42. Lim AP, et al. Neutralizing human monoclonal antibody against H5N1 influenza HA selected from a Fab-phage display library. Virol J. 2008; 5:130. [PubMed: 18957074]
43. Huang CC, et al. Structural basis of tyrosine sulfation and VH-gene usage in antibodies that recognize the HIV type 1 coreceptor-binding site on gp120. Proc Natl Acad Sci U S A. 2004; 101:2706–11. [PubMed: 14981267]
44. Luftig MA, et al. Structural basis for HIV-1 neutralization by a gp41 fusion intermediate-directed antibody. Nat Struct Mol Biol. 2006; 13:740–7. [PubMed: 16862157]
45. Chan CH, Hadlock KG, Foung SK, Levy S. V(H)1-69 gene is preferentially used by hepatitis C virus-associated B cell lymphomas and by normal B cells responding to the E2 viral antigen. Blood. 2001; 97:1023–6. [PubMed: 11159532]
46. Lee JE, et al. Structure of the Ebola virus glycoprotein bound to an antibody from a human survivor. Nature. 2008; 454:177–82. [PubMed: 18615077]
47. Kashyap AK, et al. Combinatorial antibody libraries from survivors of the Turkish H5N1 avian influenza outbreak reveal virus neutralization strategies. Proc Natl Acad Sci U S A. 2008; 105:5986–91. [PubMed: 18413603]
48. Scherer EM, Zwick MB, Teyton L, Burton DR. Difficulties in eliciting broadly neutralizing anti-HIV antibodies are not explained by cardiolipin autoreactivity. Aids. 2007; 21:2131–9. [PubMed: 18090039]
49. Selvarajah S, et al. Focused dampening of antibody response to the immunodominant variable loops by engineered soluble gp140. AIDS Res Hum Retroviruses. 2008; 24:301–14. [PubMed: 18284327]
50. Scheerlinck JP, et al. Redistribution of a murine humoral immune response following removal of an immunodominant B cell epitope from a recombinant fusion protein. Mol Immunol. 1993; 30:733–9. [PubMed: 7684820]
51. Kabsch W. Automatic processing of rotation diffraction data from crystals of initially unknown symmetry and cell constants. Journal of Applied Crystallography. 1993; 26:795–800.
52. Otwinowski, ZO.; Minor, W. Processing of X-ray diffraction data collected in oscillation mode. In: Carter, CW., Jr; Sweet, RM., editors. Methods in Enzymology, Volume 276: Macromolecular Crystallography, Part A. Academic Press; New York: 1997. p. 307-326.
53. Hwang WC, et al. Structural basis of neutralization by a human anti-severe acute respiratory syndrome spike protein antibody, 80R. J Biol Chem. 2006; 281:34610–6. [PubMed: 16954221]
54. Rodriguez R, Chinea G, Lopez N, Pons T, Vriend G. Homology modeling, model and software evaluation: three related resources. Bioinformatics. 1998; 14:523–8. [PubMed: 9694991]
55. Murshudov GN, Vagin AA, Dodson EJ. Refinement of macromolecular structures by the maximum-likelihood method. Acta Crystallogr D Biol Crystallogr. 1997; 53:240–55. [PubMed: 15299926]
56. Emsley P, Cowtan K. Coot: model-building tools for molecular graphics. Acta Crystallogr D Biol Crystallogr. 2004; 60:2126–32. [PubMed: 15572765]
57. McRee DE. A visual protein crystallographic software system for X11/Xview. Journal of Molecular Graphics. 1992; 10:44–46.
58. Laskowski RA, MacArthur MW, Moss DS, Thornton JM. PROCHECK: a program to check the stereochemical quality of protein structures. Journal of Applied Crystallography. 1993; 26:283–291.
59. Rowe T, et al. Detection of antibody to avian influenza A (H5N1) virus in human serum by using a combination of serologic assays. J Clin Microbiol. 1999; 37:937–43. [PubMed: 10074505]
60. Bullough PA, Hughson FM, Skehel JJ, Wiley DC. Structure of influenza haemagglutinin at the pH of membrane fusion. Nature. 1994; 371:37–43. [PubMed: 8072525]

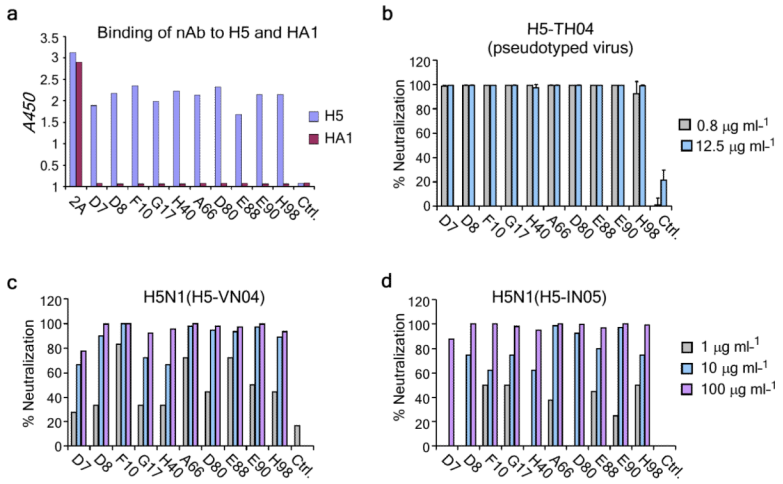

Figure 1. In vitro binding and neutralization of anti-H5 antibodies

(a) The 10 Abs were converted to soluble scFv-Fcs (scFv linked to Hinge, CH2 and CH3 domains of human IgG1) and evaluated for binding to trimeric H5-TH04 or monomeric HA1 of H5-TH04 coated on an ELISA plate. The H5 scFv-Fcs recognize trimeric H5 but not HA1. An antibody raised against HA1 ("2A") recognized both. **(b)** Neutralization of H5-TH04-pseudotyped viruses (virus-like particles with HIV-1 only cores that display H5 on their surface). % neutralization at 2 concentrations is shown with standard deviation (s.d.) bars. The mAb 80R18 was used as a negative control ("Ctrl."). **(c-d)** Neutralization of wild type H5-VN04 and H5-IN05 by the 10 scFv-Fcs at three concentrations using a plaque reduction assay. Results are consistent with those obtained from a microneutralization assay (data not shown).

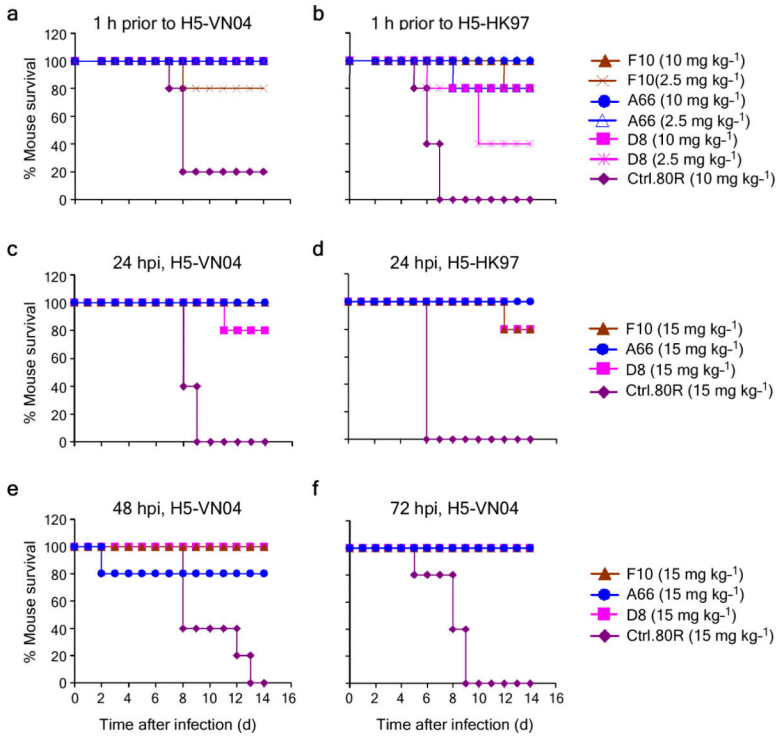

Figure 2. Prophylactic and therapeutic efficacy of anti-H5 nAbs in mice

(**a** and **b**) Prophylactic efficacy. % survival of mice treated with anti-H5 nAbs or control mAb 1h before lethal challenge by i.n. inoculation with **(a)** H5-VN04 or **(b)** H5-HK97 viruses. (**c-f**). Therapeutic efficacy. Mice were inoculated with H5-VN04 and injected with nAbs at 24, 48, 72h post-inoculation (hpi) **(c, e and f)** or with H5-HK97 at 24 hpi **(d)**.

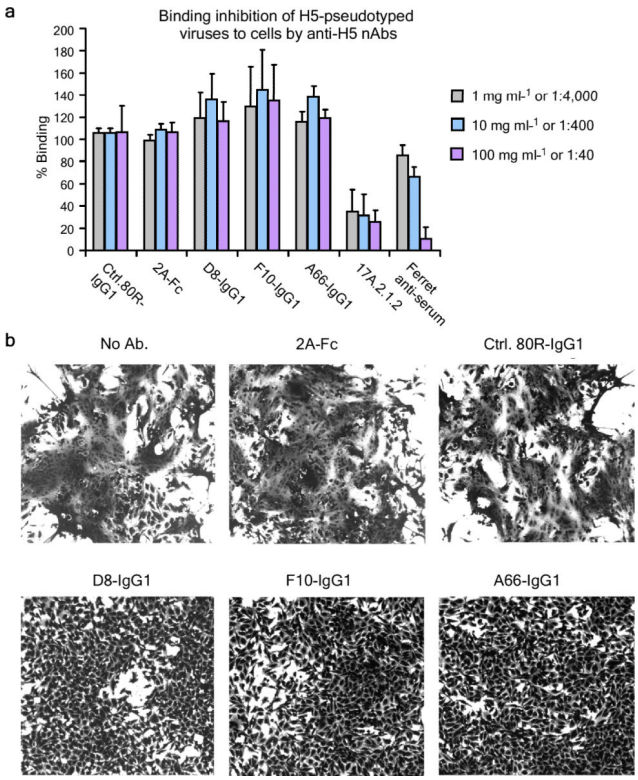

Figure 3. >Neutralization mechanism

(a) nAbs do not inhibit cell-binding of full-length HA from H5-TH04-pseudotyped HIV-1 viruses. None of the 3 nAb-treated viruses inhibited cell binding; mouse anti-H5 mAb, 17A2.1.2, and ferret anti-H5N1 serum, which inhibit haemagglutination, were used as positive controls; anti-SARS spike protein ("80R") and anti-HA1 ("2A") were used as negative controls. Vertical bars represent s.d.. **(b)** All 3 nAbs inhibit cell fusion. HeLa cells were transfected with H5-TH04-expressing plasmid and expose a pH 5.0 buffer for 4 mins in the presence or absence of nAbs. Syncytia formation induced by brief exposure to pH 5.0 was completely inhibited by D8, F10 and A66, at 20 μg ml^{-1} (~0.13μM), whereas controls ("80R" and anti-HA1 mAb ("2A") at the same concentration had no effect.

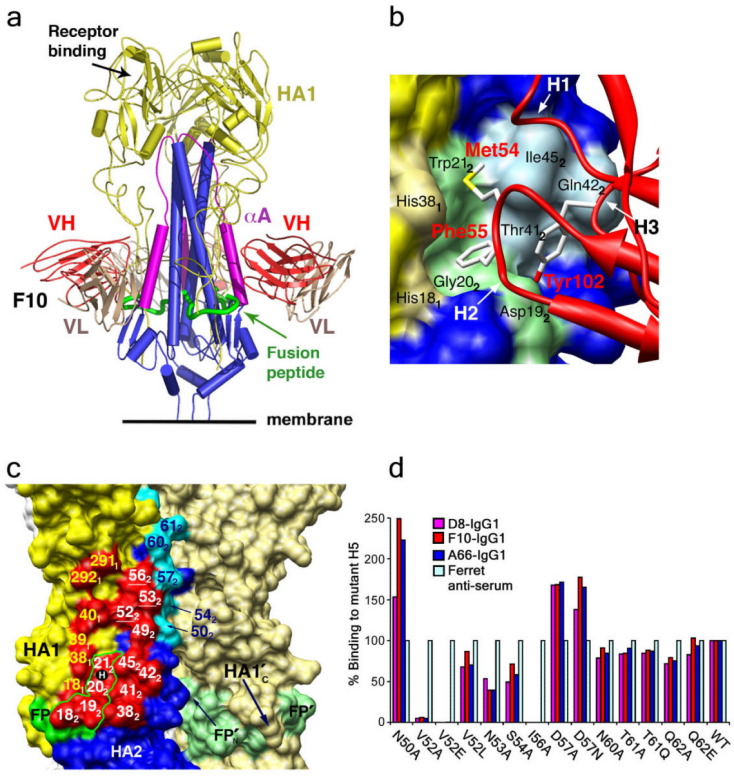

Figure 4. >Structure of the H5-F10 complex

(a) Structure of the H5 trimer bound to F10 (scFv). H5 is very similar to the uncomplexed structure35 (pairwise RMSD (Cα) = 1.0 and 0.63 Å for 2 independent trimers). HA1, HA2, the αA-helix of HA2, the "fusion peptide" (FP), and F10 (VH and VL) are color-coded. The third F10 molecule is hidden behind the stem. **(b)** Close-up of the epitope showing H5 as a molecular surface, with selected epitope residues labeled. The fusion peptide is in green. The tip of F10 (red ribbon) and selected CDR side-chains are shown. Of 1500 Å2 buried surface at the interface, 43% involves hydrophobic interactions. **(c)** Surface of the central stem region, showing two H5 monomers. One monomer has HA1 (yellow) and HA2 (blue) colored differently; the path of FP through the epitope (red) is outlined, while mutations not affecting binding are in cyan (see Fig. 4d). The fusion peptides (FP and FP') are labeled in both monomers. Epitope residues are labeled white (HA2) or yellow (HA1), the position of buried residue $H111_2$ is shown as a black ball labeled "H". **(d)** Binding of the 3 nAbs to H5 mutants in the αA helix. Note the very similar response to all mutants tested. Mutations were made either to alanine or to the corresponding H7 residue. 293T cells were transiently transfected with mutants; 24 hours after transfection, nAbs or ferret anti-H5N1 serum were used to stain the transfected cells. Mean fluorescent Intensity (MFI) was normalized against ferret anti-serum (100%) to account for different expression levels.

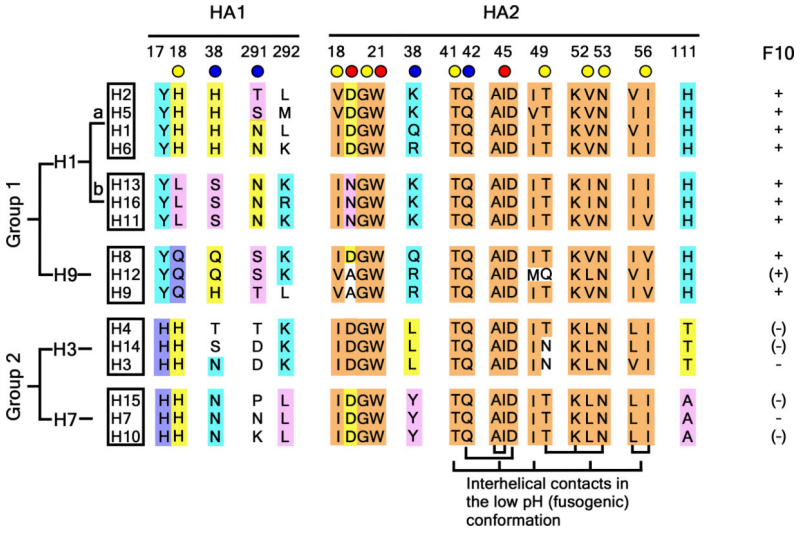

Figure 5. >Sequence conservation in HA Groups, Clusters and Subtypes at the F10 epitope

Circles below residue numbers indicate estimated contribution to the binding energy at each position: strong=red, intermediate=yellow; neutral=blue. Residues without a circle are not directly involved in the epitope but are discussed in the text. Colored highlighting on the sequences indicates conservation within clusters and groups, with orange indicating high conservation/invariance. Other colors (eg. yellow, cyan, pink) highlight residues that are cluster/subtype specific. The network of inter-helical contacts that stabilize the fusogenic structure60 are indicated below the HA2 sequences. Subtypes that can be recognized/ neutralized by F10 are indicated with "+" on the far right. "(+) or (-)" indicates a predicted positive/negative binding.

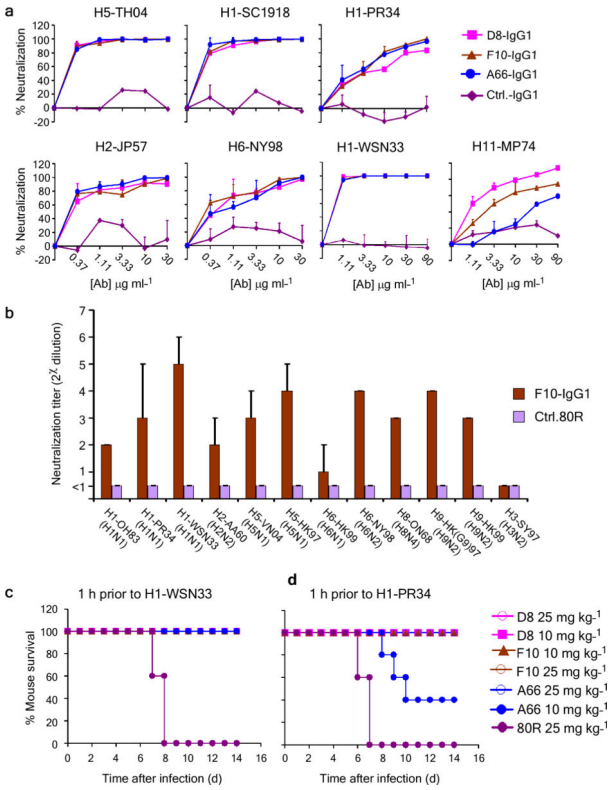

Figure 6. >Cross subtype neutralization by nAbs

(a) nAbs D8, F10 and A66 all neutralized H5-TH04, H1-SC1918, H1-PR34, H1-WSN33, H2-JP57, H6-NY98 and H11-MP74 (strains described below) pseudotyped viruses. **(b)** Microneutralization assay. Neutralization titers (0.1 mg ml^{-1} Ab stock solution) of nAb F10 against two wild-type H5N1, three H1N1, one H2N2, one H6N1, one H6N2, one H8N4, two H9N2 and one H3N2 virus. 80R is the negative control. Vertical bars and whiskers represent the lowest and highest neutralization titer (2^{χ}, values of χ are shown on the y-axis) of 2-3 independent experiments. **(c-d)** Prophylactic efficacy against two H1N1 strains in mice. % survival of mice treated with anti-H5 nAbs or control mAb are shown before lethal challenge by i.n. inoculation with **(c)** H1-WSN33 or (**d**) H1-PR34 viruses. Complete viral strain designations are: H1-OH83 (A/Ohio/83 (H1N1)), H1-PR34 (A/Puerto Rico/8/34 (H1N1)), H1-SC1918 ((A/South Carolina/1/1918 (H1N1)), H1-WSN33 (A/WSN/1933 (H1N1)), H2-AA60 (A/Ann Arbor/6/60 (H2N2)), H2-JP57 (A/Japan/305/57(H2N2)), H3-SY97 (A/Sydney/5/97(H3N2)), H6-HK99 (A/quail/Hong Kong/1721-30/99(H6N1)), H6-NY98 (A/chicken/New York/14677-13/1998 (H6N2)), H7-FP34 (A/FPV/Rostock/34 (H 7 N 1)), H 8-ON68 (A/turkey/Ontario/6118/68), H9-HK(G9)97 (A/chicken/HongKong/G9/97 (H9N2)), H9-HK99 (A/HongKong/1073/99 (H9N2)), H11-MP74 (A/duck/memphis/546/74 (H11N9)).

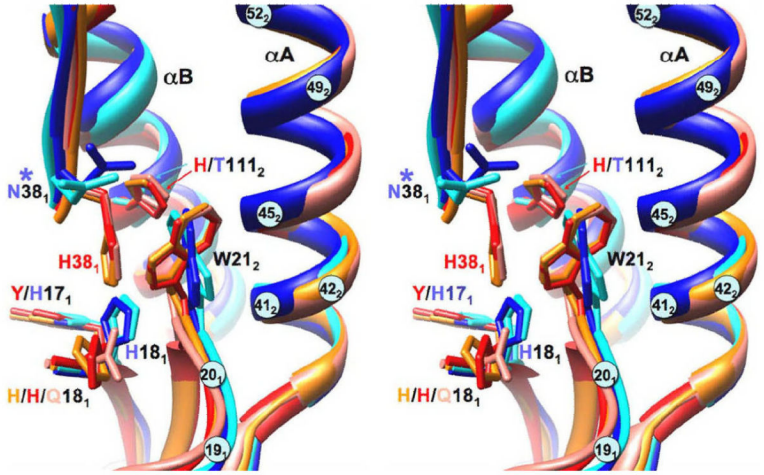

Figure 7. >3-dimensional comparison of the F10 epitope in Group 1 and Group 2 HAs

Stereo overlay of crystal structures of the 5 known HA subtypes in the region of the F10 epitope, showing conservation and differences between the 2 phylogenetic groups. H1, H5 and H9 (Group 1) are in shades of red/yellow (PDB codes 1RU7, 2IBX and 1JSD); H3 and H7 (Group 2) are in shades of blue (PDB codes 1MQL and 1TI8). RMS differences for pair-wise overlays are 0.56±0.11 Å (observed range, Group 1); 0.75 Å (Group 2); and 1.21±0.12 Å between groups. Consistent differences between phylogenetic groups include the orientation of $W21_2$ and alternative side-chain directions at 18_1 and 38_1, which are linked to the packing of buried $His111_2$ (the putative pH trigger in Group 1; absent in Group 2); and the burial of the larger tyrosine (Group 1) versus histidine (the putative pH trigger in Group 2) at 17_1. Of particular note, $N38_1$ is glycosylated in 4 members of the Group 2 clusters. Other epitope residues are indicated by numbered light blue circles.

Table 1

Data collection and refinement statistics for H5-F10.

	Native H5-F10
Data collection	
Space group	C2
Cell dimensions	
a, *b*, *c* (Å)	205., 119., 339.
α, β, γ (°)	90, 99.6, 90
Resolution (Å)	3.2(3.28-3.20) *
R_{merge}	0.13(0.81)
$I / \sigma I$	9.5(2.0)
Completeness (%)	85(68)
Redundancy	4.5(4.5)
Refinement	
Resolution (Å)	50-3.2(3.28-3.20)
No. reflections	106885
R_{work} / R_{free}	0.23(0.32)/0.29(0.38)
No. atoms	
Protein	34573
Carbohydrate	402
Water	0
B-factors	
Protein	83.5
Carbohydrate	123.7
Water	N/A
R.m.s. deviations	
Bond lengths (Å)	0.010
Bond angles (°)	1.31

A single crystal was used for both structure determination at 3.2-Å resolution and refinement.

*Values in parentheses are for highest-resolution shell.